*Earth and Planetary Science Letters*, 68 (1984) 259–270
Elsevier Science Publishers B V., Amsterdam – Printed in The Netherlands



[6]

# Tectonics of the Easter plate

Joseph F. Engeln and Seth Stein

*Department of Geological Sciences, Northwestern University, Evanston, IL 60201 (U S A )*

Received July 18, 1983
Revised version received February 14, 1984

We present a new model for the Easter plate in which rift propagation has resulted in the formation of a rigid plate between the propagating and dying ridges. We use the distribution of earthquakes, eleven new focal mechanisms, and existing bathymetric and magnetic data to describe the tectonics of this area. Both the Easter-Nazca and Easter-Pacific Euler poles are sufficiently close to the Easter plate to cause rapid changes in rates and directions of motion along the boundaries. The east and west boundaries are propagating and dying ridges; the southwest boundary is a slow-spreading ridge and the northern boundary is a complex zone of convergent and transform motion

The Easter plate may reflect the tectonics of rift propagation on a large scale, where rigid plate tectonics requires boundary reorientation. We use simple schematic models to illustrate the general features and processes which occur at plates resulting from large-scale rift propagation.

## 1. Introduction

The Easter plate is located along the Nazca-Pacific spreading center between 22° and 28° south near the location of the fastest spreading currently observed. Spreading anomalies in this area were first proposed by Herron [1], who noted that bathymetry and magnetics showed twinned spreading centers reflected in the distribution of seismicity (Fig. 1), and suggested that the oldest part of the plate was approximately 3 m.y. old. Independently, Forsyth [2] showed that earthquake focal mechanisms in this area were not consistent with Nazca-Pacific relative motion, and proposed the existence of a small plate surrounded by two ridge-transform systems. This model, further developed by Anderson et al. [3], predicts that the plate will grow with time. The southeastern and southwestern boundaries of the plate are stable spreading centers joined to the northern extension of the East Pacific Rise by long transform faults.

In contrast, using more recent marine geophysical data, Handschumacher et al. [4] interpreted the Easter plate using a propagating rift model [5,6]. In this model, the plate exists as an intermediate stage of the transfer of the plate from the Nazca to the Pacific plate. The East (Este) Ridge is propagating northward at the expense of the West (Oeste) Ridge in this model. Handschumacher et al. suggested that the Easter Plate was more complicated than simply an enlarged Galapagos [7] or Juan de Fuca [8] propagator. The poor magnetic and bathymetric signature of the southern two-thirds of the West Ridge prevented a complete tectonic analysis of the plate.

In this paper we show that the region is best described as a rigid plate which exists, at least temporarily, between the propagating and dying ridges. We then discuss more general concepts concerning rift propagation and rigid plate tectonics.

## 2. Seismicity of the Easter plate

Our tectonic interpretations are based primarily on the seismicity distribution and earthquake

0012-821X/84/$03.00 

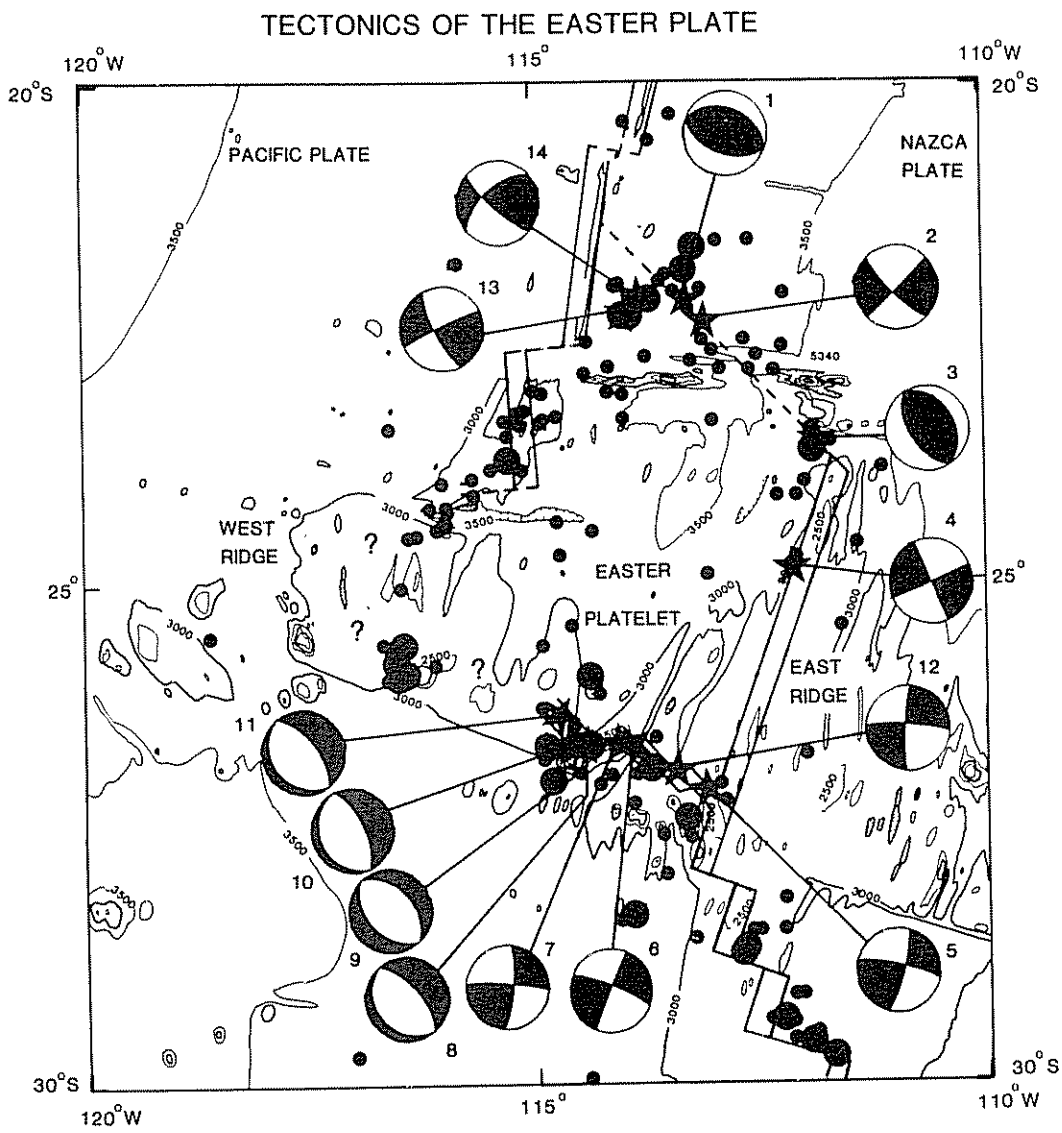


Fig. 1. Bathymetry [9], seismicity, and tectonics of the Easter plate. The dots represent earthquake epicenters listed in the NGSDC earthquake data file for the period 1963–1978 with the larger dots indicating events with $m_b > 5.1$. The stars represent earthquakes whose mechanisms have been determined; events 1 through 11 are from this study, 12 to 14 are from Forsyth [2]. The East Ridge, the northern West Ridge, and the southwest boundary are constrained by geophysical or seismological data; the other boundaries are less well known.

mechanisms. Fig. 1 shows the bathymetry of Mammerickx and Smith [9] and the earthquake epicenters. The seismicity distribution, as noted by previous workers, appears concentrated along the plate's boundaries rather than uniformly over a broad region, suggesting the existence of a rigid plate rather than a diffuse zone of deformation.

Using standard first motion, surface wave, and body wave analysis, we studied eleven earthquakes whose locations (stars) and mechanisms are shown in Fig. 1. The lack of nearby stations and stations to the west of the study area provided some difficulties in mechanism determination. For seven events, focal depths were determined using body

TABLE 1

Focal parameters, locations, and magnitudes of the events studied

| | Date | Time | Lat. | Long. | Depth [a] | $M_s$ | $m_b$ | $M_0$ | Mechanism [b] |
|---|---|---|---|---|---|---|---|---|---|
| 1 | 6/22/74 | 08:12:58 | −22.19 | −113.36 | 6 | 5.8 | 5.7 | $8\times10^{24}$ | 294/40/90 |
| 2 | 8/09/68 | 03:08:01 | −22.35 | −113.15 | 8 | 5.9 | 5.4 | $2\times10^{25}$ | 140/78/182 |
| 3 | 5/13/73 | 13:12:10 | −23.56 | −111.82 | – | 5.4 | 5.3 | $3\times10^{24}$ | 330/35/90 |
| 4 | 12/16/74 | 07:53:55 | −24.81 | −112.07 | – | 5.9 | 5.3 | $2\times10^{25}$ | 70/89/360 |
| 5 | 7/31/70 | 15:16:22 | −27.04 | −113.14 | 8 | 5.9 | 5.3 | $2\times10^{25}$ | 20/79/12 |
| 6 | 4/22/69 | 06:31:55 | −26.67 | −113.96 | – | 6.1 | 5.6 | $4\times10^{25}$ | 203/88/170 |
| 7 | 4/22/69 | 04:38:37 | −26.51 | −114.11 | 7 | 5.8 | 5.3 | $9\times10^{24}$ | 7/78/6 |
| 8 | 6/06/64 | 19:07:48 | −26.54 | −114.42 | 5 | 5.8 | 5.8 | $2\times10^{25}$ | 324/65/270 |
| 9 | 7/25/74 | 14:29:07 | −26.47 | −114.52 | – | 5.0 | 5.2 | $9\times10^{23}$ | 320/45/270 |
| 10 | 2/26/78 | 21:47:21 | −26.60 | −114.56 | 4 | 5.8 | 5.8 | $9\times10^{24}$ | 330/67/270 |
| 11 | 9/14/76 | 15:46:27 | −26.37 | −114.73 | 10 | 5.7 | 5.4 | $7\times10^{24}$ | 320/67/270 |
| 12 | 3/07/63 | 05:21:57 | −26.94 | −113.49 | | | | | 280/82/188 |
| 13 | 11/03/65 | 18:21:08 | −22.41 | −113.94 | | | 5.8 | | 65/85/165 |
| 14 | 11/06/65 | 09:22:04 | −22.17 | −113.86 | | | 5.7 | | 52/60/166 |

Events 1–11 are from this study; 12–14 are from Forsyth [2]

[a] Only depths determined using body wave analysis are indicated

[b] Strike, dip, and slip angles using Kanamori and Stewart [21] conventions.

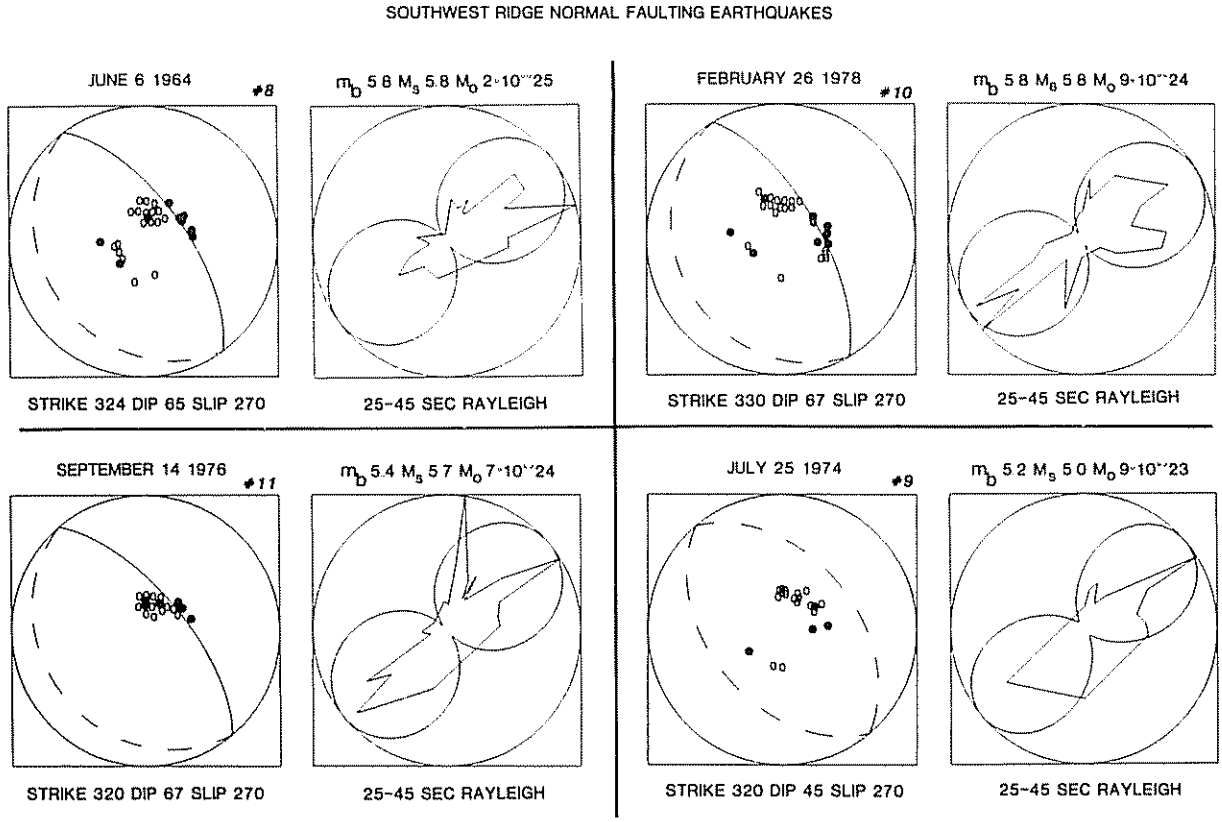


Fig. 2. Focal mechanisms (compressional arrivals solid symbols). Rayleigh wave data equalized to 90° [22] (jagged lines), and best-fitting theoretical radiation patterns for the normal faulting events on the Southwest Ridge. Uncertain nodal planes are dashed. Body wave magnitudes are from the ISC Bulletin; the surface wave magnitude and seismic moment are from this study.

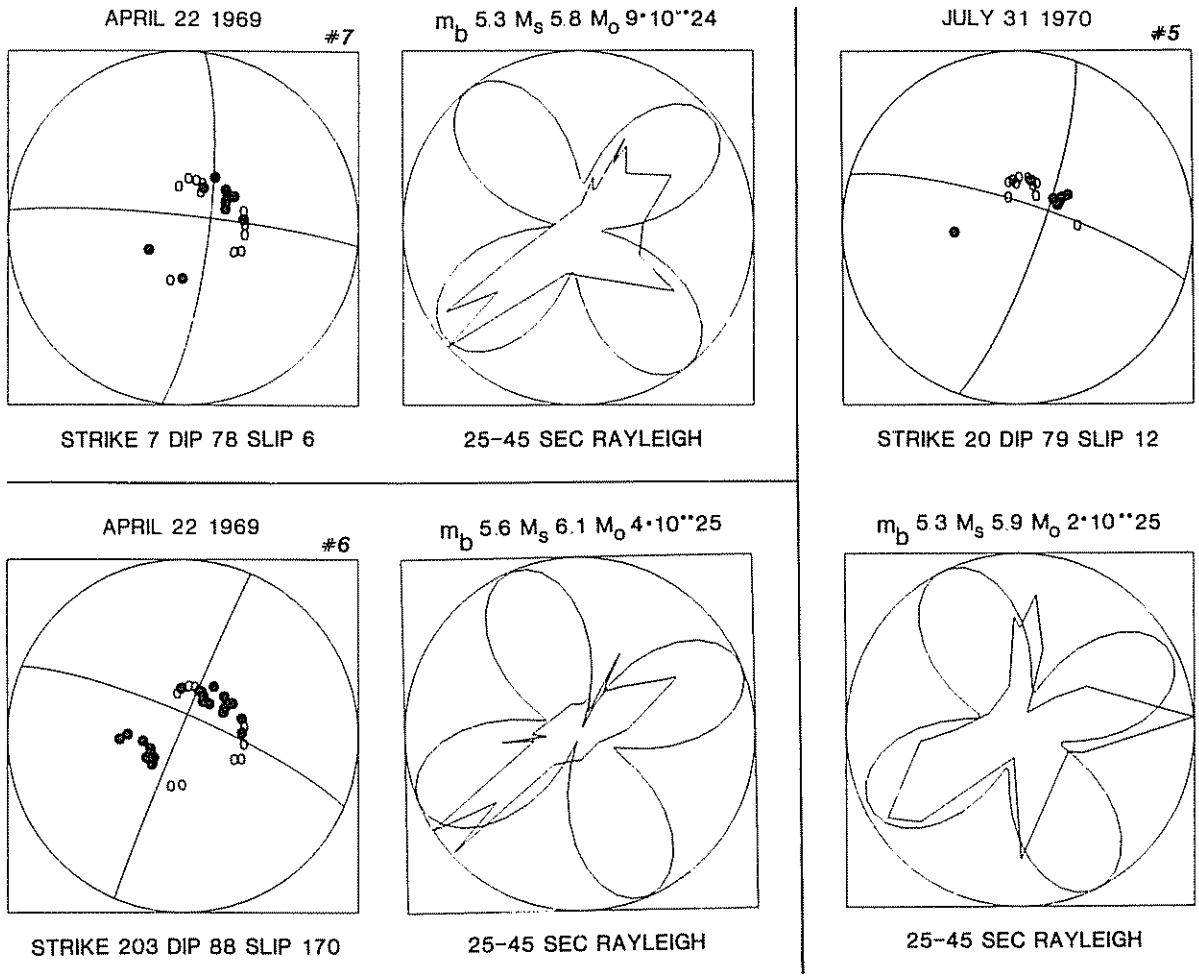


Fig. 3. Focal mechanisms and surface waves for strike-slip events on the southwest plate boundary. Earthquake 7 has a slightly different mechanism than the other two events. The poor station coverage causes lobes to the south and northwest to be poorly defined.

wave modeling with a simple water-crust-halfspace model for near-source structure [10]. All of the earthquakes examined occurred less than 9 km below the sea floor, in contrast to the ISC's reported depths of 10–85 km.

Earthquakes for which mechanisms were determined were relocated relative to event 8 (Fig. 1). This was chosen as the master event because of the large number of stations reporting, the small residuals, and the near agreement of our location and the ISC's. The changes in epicentral locations, which averaged 15 km, do not affect any tectonic interpretations. Forsyth [2] and Anderson et al. [3] published six mechanisms for earthquakes along the Easter plate's boundaries. We reexamined and slightly modified the three mechanisms determined using only first motions and used the published mechanisms for the three events previously constrained using both first motions and surface wave analysis. The focal parameters, locations, and

magnitudes of all of the events studied are listed in Table 1.

A portion of the southwest boundary is the most seismically active region around the plate. Figs. 2 and 3 show data for seven events in this area. The northeast-dipping planes of earthquakes 8 and 11 were well-constrained by P wave arrivals (Fig. 2). Events 9 and 10 were less well-constrained by the first motions, though one plane of earthquake 10 could be estimated. The surface wave radiation patterns for all four earthquakes, though poor, showed two lobes indicating primarily dip-slip faulting. All events are shown as pure normal faulting with fault planes striking in the surface wave radiation pattern nodal direction; some component of strike-slip is, of course, acceptable. Body wave modeling of earthquakes 8, 10, and 11 indicated that all occurred less than 7 km below the seafloor.

Events 5 and 7 were studied by Anderson et al. [3] using first motions; we attempted to refine the mechanisms using surface and body waves. First motions for event 6 were similar to those of event 5; the poor surface wave data did not show the four-lobed radiation pattern, presumably since there are only two stations with azimuths corresponding to two of the lobes. Event 7 has a somewhat different mechanism than the other two events. The two events for which body waves were modeled have intracrustal depths of faulting. The mechanism of earthquake 12, studied by Forsyth [2], is very similar to that of event 6 (Figs. 1, 3).

Earthquake 2 is the only well-constrained event on the northern plate boundary: first motions

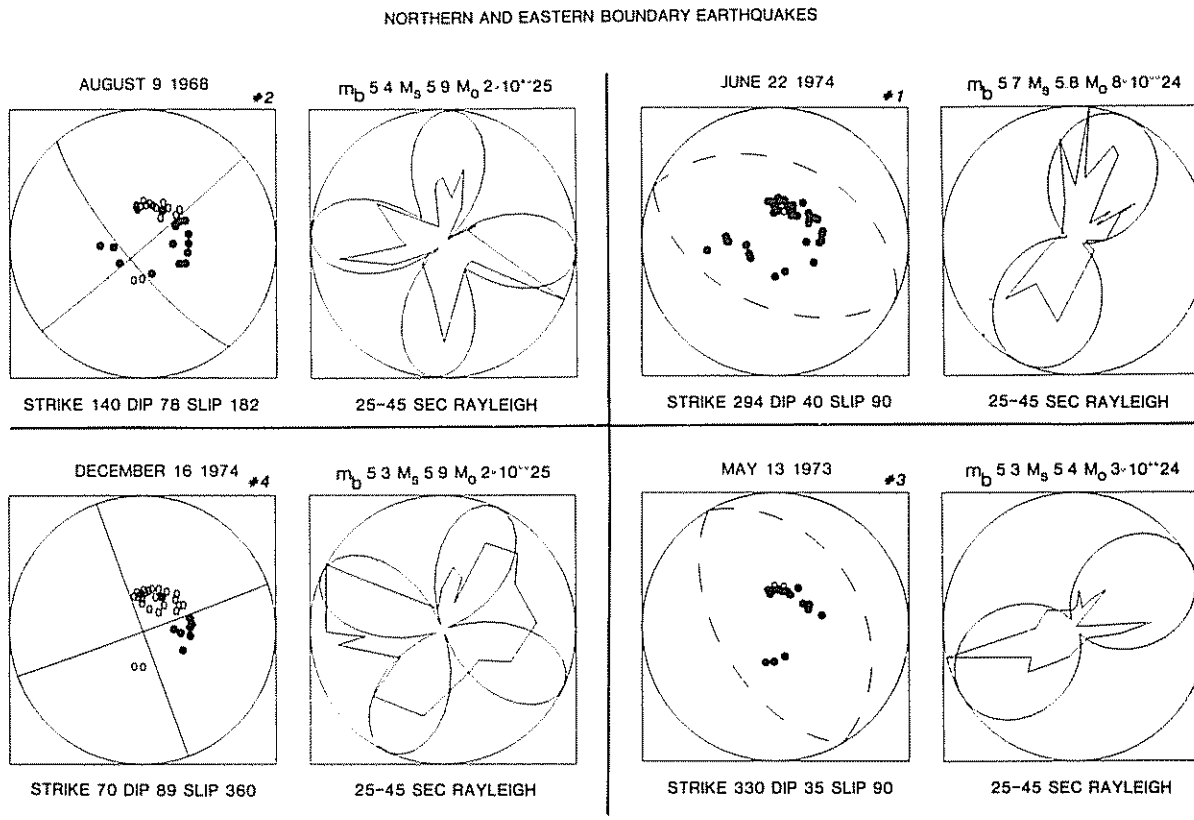


Fig. 4. Mechanisms for the earthquakes near the northern plate boundary. First motion polarities of earthquake 2 allow a strike of 129° to 140°, but the surface waves indicate that the strike is near 140°. Event 4 is a poorly constrained strike-slip event. The mechanism shown provides the best fit to the surface waves without violating the first motion data. The two predominantly thrusting earthquakes which occured along the northeast boundary are both poorly constrained and are shown as pure thrust faulting. Up to 30° of strike slip motion is allowed by the data; neither nodal plane could be determined.

limited the northwest-trending plane's strike to 309° to 320° and the surface waves favored a strike near 320° (Fig. 4). Event 4 is reasonably well constrained by first motions but the surface wave fit is poor. The nodal planes for events 1 and 3 could not be well determined. Both have significant thrust components, as shown by compressional first motions and two-lobed Rayleigh wave patterns, and were drawn as pure thrust with fault planes in the Rayleigh wave nodal directions, though up to 30° of strike-slip motion can be accommodated without introducing a large radiation pattern misfit or violating the first motion polarities.

## 3. Tectonics

We combined the seismicity distribution and mechanisms with marine geophysical data to form a regional tectonic model (Fig. 1). The East Ridge is well defined bathymetrically and has been shown to be rapidly spreading by Handschumacher et al. [4] (Fig. 5). The low level of seismicity along the ridge crest is as expected for a fast-spreading ridge. The southwest boundary is the most active seismically. The normal faulting events suggest slow spreading, by analogy to the Mid-Atlantic Ridge; whereas the strike-slip events suggest transform motion. The limited magnetic data show that the northwest boundary is spreading rapidly. The nature of the northeast boundary, on which both thrust and strike-slip motions occur, is not obvious. We assumed that the northeast boundary could be roughly defined by the seismicity, although this trend crosscuts several structures and has no clear bathymetric expression. This boundary may be a diffuse deformation zone as we will discuss later. The central portion of the west boundary is even more obscure due to the absence of significant seismicity and morphologic expression.

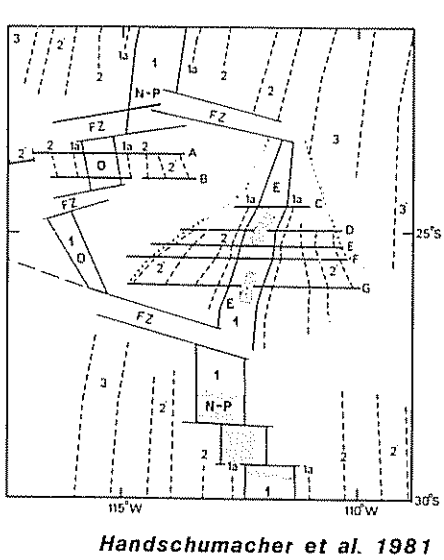


Fig. 5. Magnetic anomalies in the Easter plate region [4]. In their interpretation, the fanning of anomalies and the absence of anomalies older than 1a on track C indicate that the East Ridge is a propagating rift

Since the seismicity distribution suggested that the Easter plate could be treated as essentially rigid, we attempted to determine relative motions between the Easter, Nazca, and Pacific plates by inverting for Euler vectors using our implementation of Minster et al.'s [11] algorithm. We used two types of data along the Easter plate boundaries. Spreading rates were estimated using Handschumacher et al.'s [4] identification of magnetic anomaly 1a (0.94 m.y. B.P.) at three points on the East Ridge and at one point on the West Ridge (Fig. 5). Because the bathymetric data (Fig. 1) are inadequate to resolve transform fault orientations on either ridge, rates were measured perpendicular to the ridge axis. We also used slip vectors from all events shown in Fig. 1 except those on the northeast boundary (whose tectonic significance is unclear). No significant change in the location of the poles occurred if the predominantly strike-slip events from this boundary were included.

For Nazca-Pacific motion we used the data and uncertainties of Minster and Jordan [12], except for two earthquakes which occur on the Pacific-Easter boundary in our model. This deletion changed the Nazca-Pacific pole about one degree from Minster and Jordan's best fit pole. Their magnetic data average over a longer time period, about 3 m.y., than the Easter plate data. All the inversion data are listed in Table 2; Fig. 6 shows the locations of the data points on the Easter plate

TABLE 2

Plate motion data

| Lat | Long | Datum | Standard deviation | Weighted residuals [a] |
|---|---|---|---|---|
| *Nazca–Pacific (NZ-PA)* | | | | |
| *Rates* | | | | |
| −5.80 | −106.80 | 15.30 | 0.8 | 0.03 |
| −9.40 | −110.00 | 16.30 | 0.8 | 0.62 |
| −9.90 | −110.10 | 15.50 | 0.8 | −0.45 |
| −10.80 | −110.30 | 16.60 | 1.0 | 0.64 |
| −11.40 | −110.50 | 16.10 | 1.0 | 0.07 |
| −12.00 | −110.80 | 15.90 | 0.6 | −0.33 |
| −19.00 | −113.00 | 16.50 | 1.0 | −0.20 |
| −20.00 | −113.80 | 16.10 | 0.6 | −1.13 |
| −28.00 | −112.00 | 17.50 | 0.8 | 0.54 |
| *Transforms* | | | | |
| −3.70 | −102.90 | s81e | 3.0 | 0.52 |
| −4.50 | −105.50 | s78e | 3.0 | 0.52 |
| −6.00 | −107.00 | s73e | 5.0 | −0.84 |
| −13.50 | −112.00 | s70e | 10.0 | −0.51 |
| *Slip vectors* | | | | |
| −4.40 | −105.90 | s75e | 20.0 | −0.13 |
| −4.50 | −106.00 | s76e | 15.0 | −0.11 |
| −4.60 | −105.80 | s77e | 15.0 | −0.05 |
| −13.30 | −111.50 | s75e | 20.0 | −0.02 |
| −28.70 | −112.70 | s62e | 20.0 | −0.67 |
| *Nazca–Easter (NA-EA)* | | | | |
| *Rates* | | | | |
| −26.41 | −112.72 | 11.60 | 1.0 | −1.00 |
| −25.38 | −112.28 | 10.20 | 1.0 | 0.11 |
| −24.38 | −111.93 | 9.40 | 1.0 | 1.57 |
| *Slip vectors* | | | | |
| −22.35 | −113.15 | s40e | 20.0 | −0.16 |
| −24.81 | −112.07 | n70e | 20.0 | 1.37 |
| *Easter–Pacific (EA-PA)* | | | | |
| *Rates* | | | | |
| −23.36 | −115.42 | 12.20 | 1.0 | 0.75 |
| *Slip vectors* | | | | |
| −26.67 | −113.96 | s71e | 20.0 | −1.44 |
| −26.51 | −114.11 | n77e | 20.0 | 0.00 |
| −26.59 | −114.42 | n54e | 20.0 | 0.71 |
| −27.04 | −113.14 | s72e | 20.0 | 0.06 |
| −26.57 | −114.52 | n50e | 20.0 | 0.80 |
| −26.37 | −114.73 | n50e | 20.0 | 0.68 |
| −26.60 | −114.56 | n60e | 20.0 | 0.23 |
| −22.13 | −113.76 | s45e | 20.0 | 0.75 |
| −22.34 | −113.98 | s26e | 20.0 | −0.28 |
| −26.87 | −113.58 | s72e | 20.0 | −0.79 |

[a] Weighted residuals are those for the inversion using all the data and no assumption of orthogonality.

TABLE 3

Euler vectors

| | Lat | Long | deg/m.y. | Reduced chi-squared |
|---|---|---|---|---|
| *All data* | | | | |
| NZ-PA | −55.2 | 93.3 | 1.5 | |
| EA-NZ | −20.9 | −111.5 | 11.6 | |
| EA-PA | −28.3 | −113.6 | 11.4 | |
| | | | | 0.550 |
| *All data (assumed orthogonal spreading)* | | | | |
| NZ-PA | −53.2 | 92.8 | 1.6 | |
| EA-NZ | −20.6 | −111.1 | 10.6 | |
| EA-PA | −28.7 | −113.5 | 10.3 | |
| | | | | 0.644 |
| *All NZ-PA data; EA rates only (assumed orthogonal spreading)* | | | | |
| NZ-PA | −52.6 | 91.7 | 1.6 | |
| EA-NZ | −20.0 | −110.2 | 9.0 | |
| EA-PA | −29.6 | −112.9 | 8.8 | |
| | | | | 0.510 |
| *All NZ-PA data; EA rates only* | | | | |
| NZ-PA | −55.8 | 94.2 | 1.5 | |
| EA-NZ | −18.3 | −105.7 | 5.7 | |
| EA-PA | −33.5 | −109.3 | 5.5 | |
| | | | | 0.273 |

boundaries. We assigned all the Easter plate spreading rates an uncertainty of 10 mm/yr, and the slip vectors an uncertainty of 20 degrees.

Four separate inversions using all Nazca-Pacific data and different subsets of Easter data were carried out, yielding the results listed in Table 3. First, all data were used, yielding the poles shown by stars and relative motions shown by arrows in Fig. 6. Next, fictitious transforms were added at the sites of the four rate measurements on the Easter plate boundaries, as a method of enforcing orthogonal spreading. The resulting poles are indicated by the large circles. The final two inversions did not include any slip vector data along the Easter plate boundaries. In one case only the four rate data were used; in the other, fictitious orthogonal transforms were added at these sites.

The inversion results (Fig. 6) seem reasonable. Both EA-NZ and EA-PA poles are quite near the plate, allowing significant variation in relative motion along the boundaries. Since the spreading rate decreases rapidly to the north along the East Ridge,

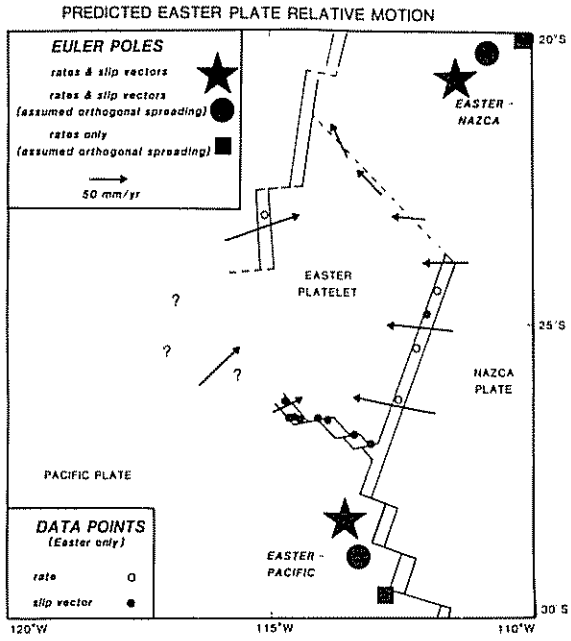


Fig. 6. Rigid plate analysis of the Easter plate system showing the Euler poles for different subsets of the data. The motions of the Easter plate relative to the Nazca and Pacific plates predicted using all of the data are indicated by the arrows. The open and closed circles represent the locations of rate of slip vector measurements.

the EA-NZ pole is essentially along the strike of the ridge. The EA-PA pole, to the south, fits the observed spreading rate on the northwest boundary, and predicts slow spreading on the southwest boundary. The transform direction implied by the strike-slip events on the southwest boundary is fit well by the predicted motions and spreading here is predicted to be slightly oblique from the normal faulting nodal directions.

The predicted relative motions are similar for the four different inversions (Fig. 6). The poles resulting from the inversion which used only the Easter spreading rates and no assumed orthogonality differ most from the other three inversions. (This inversion's poles fall slightly off the map in Fig. 6 and thus are not shown.)

The values of chi-squared (Table 3) indicate that the data contain some errors as well as possible deviations from plate rigidity. Despite the lower value of reduced chi-squared obtained by deleting all Easter plate azimuthal data, we consider the poles resulting from inclusion of the azimuthal data a better description of a complex situation. We consider the Easter plate rigid to a reasonable approximation.

The seismicity along the northeast boundary (or diffuse boundary zone) indicates the complexity of this feature caused by the proximity of the pole of rotation, the length and overall trend of this boundary, and the nearly continuous migration of this feature. As shown in Fig. 6, this boundary has a predicted relative motion which changes from oblique convergence to strike-slip to oblique divergence from west to east. The exact tectonics and geometry of this boundary can not be determined with the data presently available. The predicted relative motions are roughly consistent with all but one of the earthquake mechanisms although, without better bathymetric control, the relation of the mechanisms to the relative motions can not be resolved. Event 3 may be related to some structural or geometric complexity near the eastern end of this boundary or may be caused by compression ahead of the propagating rift tip in a manner similar to that suggested by Hey et al. [6].

## 4. Discussion

The present plate geometry can evolve in at least two different ways. If the West Ridge continues spreading, the Easter plate will grow as suggested by Anderson et al. [3]. However, if the West Ridge dies, the Easter plate will be transferred from the Nazca to the Pacific plate as in previously studied areas of rift propagation [7,8].

The spreading rate predicted by our inversion for the northernmost site of spreading on the East Ridge (which may be regarded as the propagating rift tip) is 60 mm/yr. Thus, either no slower spreading has developed or propagation has been stopped for some reason. Perhaps the propagator has encountered a fracture zone and requires some time to break through. Alternatively, if propagation is episodic, we may be observing a period of no propagation. Finally, the East Ridge has been propagating into older crust than previously studied propagators; perhaps the cooler, stronger, and thicker lithosphere has been retarding propagation.

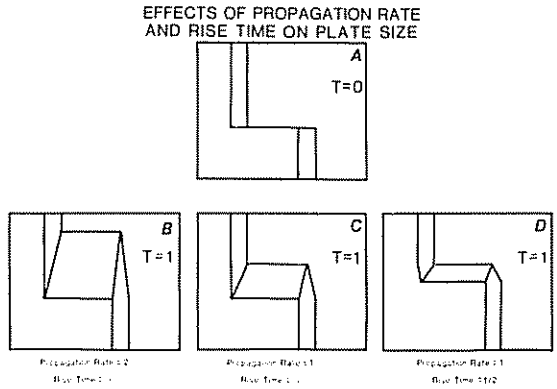


Fig 7 Simple models which show the effects of propagation rate and rise time on plate size. Fig. 7A is the pre-propagation geometry; B through D show the same area at the same later time. The area between the ridges is either a plate or shear zone. A larger propagation rate (B) results in a larger plate, a shorter rise time lessens plate size (D).

The evolution of the Easter plate to its present geometry can not be determined from the current relative motions without better bathymetric and magnetic data. Because the data are insufficient to permit actual reconstructions, we explored the evolution of such a plate using a simple model. In this model, three factors influence the size of the area between the propagating and dying ridges (Fig. 7). The "rise time" (which we define as the interval from the inception of spreading until full spreading is reached at any point along the propagating fit) and the propagation rate determine the length of ridge overlap. The offset between the ridges determines the length of the shear or transform faults which may develop.

Fig. 7A sows a simple pre-propagation plate geometry with two orthogonally spreading ridges offset by a transform fault. Fig. 7B, C, and D show the same area at some time later. The ridges away from the plate produced are held fixed. Fig. 7C shows the geometry resulting from a propagation rate and rise time arbitrarily set at 1. The area between the overlapping ridges may be either a rigid plate or a diffuse shear zone. If the propagation rate doubles while the rise time stays constant, the plate area doubles (Fig. 7B). However, if the propagation rate is the same as that in Fig. 7C and the rise time is halved, the plate area is halved (Fig. 7D). Thus, the product of the propagation rate and rise time determines the overlap length. The effect of offset would simply be to change the horizontal scale of the figure. The product of these three factors yields the area of the plate or shear zone produced for this simple model.

In this model, either a rigid plate or diffuse shear zone can result as the rift propagates, ultimately transferring crust from one plate to another. Perhaps these two cases are the limits of a con-

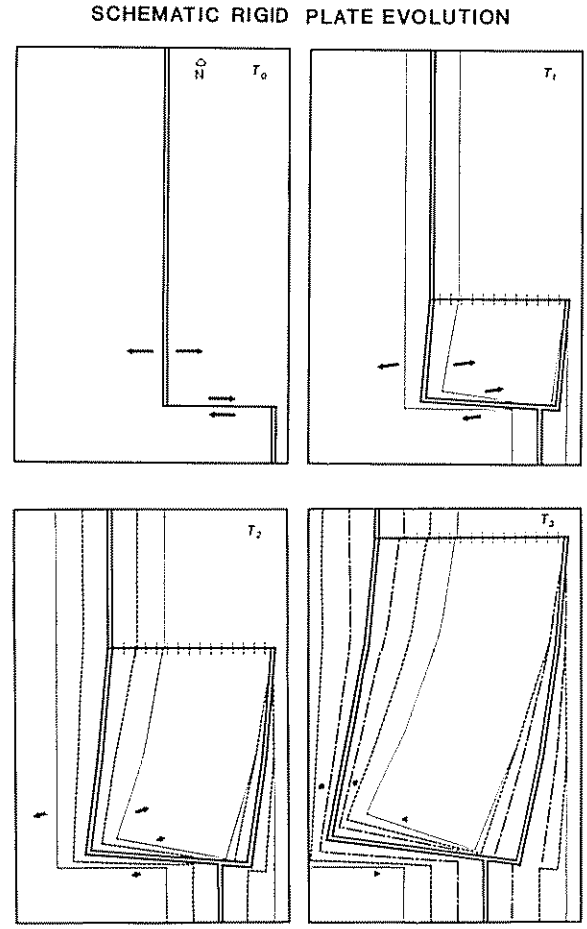


Fig 8 Schematic rigid plate evolution. The propagating rift spreads orthogonally and reaches full spreading at its base at time $T_3$. Spreading on the dying ridge becomes more oblique (arrows) while the transform changes into a ridge which approaches orthogonal spreading over time. The difference in spreading rate at the base of the propagator offsets the propagating rift from the pre-existing ridge. The northern boundary is a zone of compression which migrates along with the propagating tip.

tinuum for which the controlling variable may be the size of the area between the two ridges. The overlapping spreading centers of Macdonald and Fox [13] would be an example of small-scale propagation with short ridge overlaps and offsets, characterized by the formation of shear zones in the overlap areas. The Easter plate would represent large-scale propagation, where the large area between the overlapping ridges resists shearing and a plate obeying rigid plate tectonics forms. Fig. 8 illustrates the schematic evolution of such a plate for a very simple geometry not meant to be directly applicable to the Easter plate, but which shows strong similarities.

Prior to the initiation of propagation ($T_0$), the ridges are spreading symmetrically and orthogonally. The Euler pole for this plate pair is very distant and the plate to the east will be held fixed. The eastern ridge segment propagates northward with time. The Euler pole for the plate to the east and the plate between the overlapping ridges is at the propagating tip (so that the spreading rate here is zero) and the third pole for this system was determined by closure. We have divided the propagation process into three steps with full spreading reached at the site of earliest propagation at time $T_3$. Continuous propagation would not change these results except to smooth the changes in ridge and anomaly orientations

As a new spreading center develops, the old spreading center adjusts to keep the total spreading rate and direction constant between the two large plates. Since the propagating rift spreads orthogonally, the dying ridge not only slows its rate but also changes spreading direction. Relative motion across the original transform also changes during propagation. Since motion of the small plate relative to the western plate is no longer parallel to this boundary, the transform evolves into a "leaky" transform [14] and then into a nearly orthogonally spreading ridge.

The northern plate boundary is the most difficult to interpret. The location of this boundary changes continuously if propagation is continuous, but is always the site of compression. We have connected the propagating tip to the dying ridge with the shortest possible boundary; the point of intersection of the northern boundary and the dying ridge is arbitrary. It would be difficult for true subduction to develop because the crust on both sides of this boundary is very young and this feature migrates nearly continuously; perhaps a broad zone of deformation develops.

Because finite time is taken to reach full spreading on the propagating rift, an offset develops between the propagator and the ridge from which it grew. The offset length is determined by the difference in spreading rate on either side of the offset while the propagator approaches full spreading. If the rise time is short and the propagator has a rapid early change in spreading rate, the offset is short. In this model, the acceleration of spreading is nearly constant so the offset is approximately one-fourth of the full spreading rate times the rise time. The relative northward motion of the original transform boundary caused by the initiation of spreading on this boundary, causes the southern triple junction to migrate northward.

Some of the features of our schematic plate evolution are similar to those observed at the Easter plate. Since this is a general model for which we know all of the inputs, a comparison of this and the real plate system should yield insights into the Easter plate system. For example, the orientation of the active ridge segments could have resulted from several possible geometries, which are illuminating to discuss.

In our simple model, the iniation of spreading on and the differential spreading rates along the propagating rift cause the overall trend of the dying ridge to be rotated clockwise. However, the relative motion across this boundary changes from east-west to northeast-southwest with time (Fig. 8). Since the transforms must remain parallel to the direction of relative motion, any transforms along this ridge must reorient progressively counter-clockwise thus cutting across previous trends. Ridge segments may either spread with increasing obliquity or rotate counter-clockwise to remain nearly normal to the spreading direction. Handschumacher et al. [4] could not determine the location or orientation of much of the central and southern West Ridge because of its poor magnetic and bathymetric signature, which they inferred was caused by closely spaced fracture zones. The overprinting of transform orientations produced as

propagation continued is an alternative explanation. Individual ridge segments may have also reoriented although we do not know the details of the history of the West Ridge.

Because the southwest boundary's orientation is close to that of the Nazca-Pacific transforms, the most plausible explanation is that a Nazca-Pacific transform has evolved into a slowly spreading ridge as in the simple model (Fig. 8). Alternatively, to produce the present geometry from a Nazca-Pacific ridge segment requires a rotation of both ridge and transform segments of approximately 50° counter-clockwise, assuming that spreading was orthogonal prior to propagation.

Spreading on the East Ridge is predicted to be nearly orthogonal (Fig. 6) and this ridge's geometry is similar to that of the propagator in our schematic model. No large offset has been measured at the southern triple junction of the Easter plate, though this area's geometry is not well determined. A linear increase in spreading rate on the propagating East Ridge would have resulted in an offset of greater than 100 km, suggesting that a rapid acceleration of spreading characterized the early history of this propagator.

As in the schematic model, the northeast boundary connecting the propagating tip to the dying ridge is the most complex. Because the Easter-Nazca pole is not at the propagating tip, parts of this boundary are not under compression. This boundary, or deformation zone, is oriented so the amount of compression across the boundary is much less than along the equivalent model boundary. This boundary may evolve toward a pure transform boundary but cannot reach that geometry because of continued propagation.

Comparison of this model with the Easter and Galapagos situations suggests that the dominant factor determining the behavior of the area between the ridges is the size of this area. The more lithosphere that is present, the more difficult it is for this area to be sheared. Thus, while small-scale ridge overlaps appear to have extensively sheared regions between the ridges [13], large-scale propagation will tend to produce rigid plates.

Evidence for similar plates appears to be preserved in magnetic anomalies in the ocean floor. Mammerickx et al. [16] showed that between 8.2 and 6.5 m.y. ago a small plate existed between the East Pacific Rise and the then-active Galapagos Rise. They inferred from magnetic and bathymetric data that the East Pacific Rise was a slow spreading ridge at the plate's western boundary until spreading stopped on the Galapagos Rise and the plate was transferred to the Nazca plate. Similarly, Cande et al. [17] proposed that a plate existed temporarily at the Farallon-Aluk-Antarctic-Pacific junction about 45 m.y. ago. This plate was formed because of rift propagation and resulted in the transfer of the plate from the Pacific to the Antarctic plate.

At present, little is understood about spreading center reorientations, whether on a regional or small scale. A wide variety of features including the non-transform offset at 20.8°S [15], numerous twinned spreading centers separated by 2 to 20 km [13], and the "Lower" [1] or "Juan Fernandez" [18] plate near the Pacific-Nazca-Antarctic triple junction show that perturbations from simple spreading center geometry are common along the ridges of the eastern Pacific. Presumably, in some complex way, these phenomena are related to the high spreading rate, changes in relative motion, of other local factors.

Since this paper was written, new geophysical studies have been conducted in this region. Analysis of this data, now underway [19,20], should provide details of the present geometry and evolution of the Easter plate beyond those that could be determined with our data set.

## Acknowledgements

We thank Richard Gordon, Donna Jurdy, Doug Wiens, Laurel Henderson, Jean Francheteau, and Jason Phipps Morgan for valuable discussion of this work. The plate motion inversion program used was written jointly by Richard Gordon and Seth Stein. We also thank Richard Hey and two anonymous reviewers for their helpful comments.

This research was supported by NSF grants EAR 8007363 and EAR 8206381, NASA Crustal Dynamics Contract NAS5-27238, a Cotrell Research Grant, and the Petroleum Research Fund of the American Chemical Society.

## References


1 E M Herron, Two small crustal plates in the South Pacific near Easter Island, Nature 240, 35–37, 1972.

2 D W Forsyth, Mechanisms of earthquakes and plate motions in the east Pacific, Earth Planet Sci Lett 17, 189–193, 1972.

3 R N Anderson, D W Forsyth, P Molnar and J Mammerickx, Fault plane solutions of earthquakes on the Nazca plate boundaries and the Easter plate, Earth Planet Sci Lett 24, 188–202, 1974.

4 D W Handschumacher, R H Pilger, Jr., J A Forman and J F Campbell, Structure and evolution of the Easter Plate, in: Nazca Plate: Crustal Formation and Andean Convergence, L D Kulm, J Dymond, E J Dasch and D M Hussong, eds., Geol Soc Am Mem 154, 63–76, 1981.

5 R N Hey, A new class of pseudofaults and their bearing on plate tectonics: a propagating rift model, Earth Planet Sci Lett 37, 321–325, 1977.

6 R N Hey, F K Dunnebier and W J Morgan, Propagating rifts on mid-ocean ridges, J Geophys Res 85, 3658–3674, 1980.

7 R N Hey and P R Vogt, Spreading center jumps and sub-axial asthenosphere flow near the Galapagos hotspot, Tectonophysics 37, 41–52, 1977.

8 R N Hey and D S Wilson, Propagating rift explanation for the tectonic evolution of the northeast Pacific—the pseudomovie, Earth Planet Sci Lett 58, 167–188, 1982.

9 J Mammerickx and S M Smith, Bathymetry of the Southeast Pacific, Geol Soc Am, Map and Chart Ser MC-26 442, 194, 1978.

10 G C Kroeger and R J Geller, An efficient method for synthesizing teleseismic body waves for shallow sources in a vertically stratified medium, J Geophys Res (in press).

11 J B Minster, T H Jordan, P Molnar and E Haines, Numerical modeling of instantaneous plate tectonics, Geophys J R Astron Soc 36, 541–576, 1974.

12 J B Minster and T H Jordan, Present day plate motions, J Geophys Res 83, 5331–5354, 1978.

13 K C Macdonald and P J Fox, Overlapping spreading centers: new accretion geometry on the East Pacific Rise, Nature 302, 55–58, 1983.

14 H Menard and T Atwater, Changes in the direction of seafloor spreading, Nature 219, 463–467, 1968.

15 D K Rea, Asymmetric sea-floor spreading and a nontransform axis offset: the East Pacific Rise 20°S survey area, Geol Soc Am Bull 89, 836–844, 1978.

16 J Mammerickx, E Herron and L Dorman, Evidence for two fossil spreading ridges in the southeast Pacific, Geol Soc Am Bull 91, 263–271, 1980.

17 S C Cande, E M Herron and B R Hall, The early Cenozoic history of the southeast Pacific, Earth Planet Sci Lett 57, 63–74, 1982.

18 H Craig, K R Kim and J Francheteau, Active ridge crest mapping on the Juan Fernandez micro-plate: the use of Seabeam-controlled hydrothermal plume surveys, EOS Trans Am Geophys Union 64, 856, 1983.

19 R N Hey, D F Naar, M C Kleinrock, E Morales and L Johnson, Micro-plate tectonics and fast rift propagation along the superfast spreading East Pacific Rise near Easter Island, EOS Trans Am Geophys Union 64, 855, 1983.

20 D F Naar and R N Hey, Preliminary analysis of Seabeam and magnetics data from the Easter microplate, EOS Trans Am Geophys Union 64, 855, 1983.

21 H Kanamori and G S Stewart, Mode of strain release along the Gibbs Fracture Zone, Mid-Atlantic Ridge, Phys Earth Planet Inter 11, 312–332, 1976.

22 H Kanamori, Synthesis of long period surface waves and its application to earthquake source studies; the Kurile Islands earthquake of October 13, 1963, J Geophys Res 75, 5011–5027, 1970.